ORIGINAL PAPER

Synthesis and characterization of graphene and ordered mesoporous TiO$_2$ as electrocatalyst for the determination of azo colorants

Tian Gan · Junyong Sun · Haijing Zhu · Jianjun Zhu · Degong Liu

Abstract Ordered mesoporous TiO$_2$, synthesized by soft template method, coupled with graphene was used to modify a carbon paste electrode. The graphene layer was very thin and the mesoporous TiO$_2$ particles were nano-scale, as confirmed by scanning electron microscopy and transmission electron microscopy. Graphene and mesoporous TiO$_2$ displayed remarkable enhancement effect and greatly increased the oxidation signals of two azo colorants, i.e., Ponceau 4R and Allura Red. The influence of electrolyte, scan rate, amount of graphene and mesoporous TiO$_2$, accumulation potential, and time on the signal enhancement of Ponceau 4R and Allura Red was discussed, and therefore, a novel and sensitive electrochemical method was developed for the detection of Ponceau 4R and Allura Red. The linear range was wider than two order of magnitude for both of Ponceau 4R and Allura Red. The limit of detection for Ponceau 4R and Allura Red was 1.35 and 0.34 nM, respectively. Finally, this method was successfully applied in soft drink and sausage samples, which was confirmed by high-performance liquid chromatography technique.

Keywords Ponceau 4R · Allura Red · Graphene · Mesoporous TiO$_2$ · Electrochemical determination

Introduction

Graphene is a single-atom thick, two-dimensional material that has attracted great attention due to its good mechanical, electrical, and thermal properties [1, 2], and it has received considerable attention recently. It has large surface area-to-volume ratio and good chemical stability and thus can be used as adsorbent [3], ultra-capacitor material [4], or support structure for the development of heterogeneous catalysts with enhanced activities [5]. Graphene-based supports for metal or metal oxide nanoparticles have been demonstrated to exhibit high efficiencies for cancer biomarker [6], antibiotics [7], H$_2$O$_2$ [8], and environmental pollutants [9].

Mesoporous molecular sieves were first prepared by scientists at Mobil Oil Research and Development in 1992 [10, 11], which are characterized by their high surface area. These materials are of very great interest in catalysis because of their large and uniform pore sizes. Among them, nanostructured mesoporous metal oxides are a class of sensing materials with wide application prospect in catalysis, gas separation, ion exchange, and possibly would display fascinating electronic, optical, magnetic, photochemical, and/or electrochemical behavior [12, 13]. For example, mesoporous TiO$_2$ has been shown to be potentially advantageous because it shows higher surface areas, much more uniform and controllable pore size, and pore morphologies compared to randomly organized nanocrystalline TiO$_2$ [14].

Synthetic colorants, a very important class of food additives, are added to food products to make them more attractive, replacing their natural color that can be lost during the industrial processes. Ponceau 4R (Scheme 1a) and Allura Red (Scheme 1b) are two of these colorants, which can provide red color to many common food products. However, Ponceau 4R and Allura Red pose potential risks to human health because they have azo structure, especially if they are excessively consumed [15]. Consequently, the use of synthetic azo colorants in food products is strictly controlled by different national legislations. For example, the maximum allowable usage amount of Ponceau 4R and Allura Red in China is 0.5 and 0.085 g kg^{-1}, respectively. Therefore, the development of determination method for them is very important and significant. Recently, the electrochemical methods with the merits of easy fabrication, low cost, fast response, and no need for

T. Gan (✉) · J. Sun · H. Zhu · J. Zhu · D. Liu
College of Chemistry and Chemical Engineering, Xinyang Normal University, Xinyang 464000, People's Republic of China
e-mail: gantianxynu@163.com
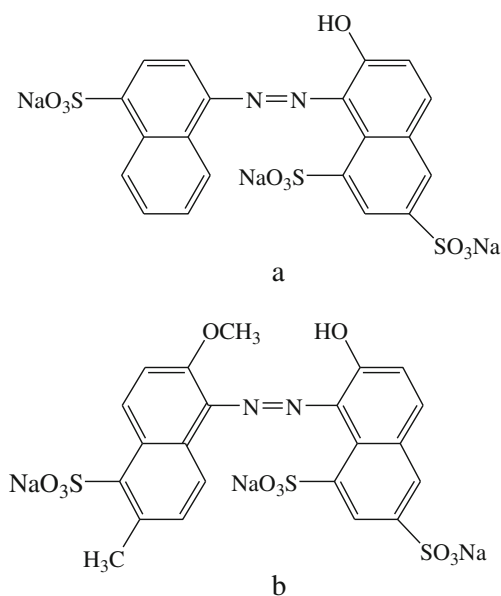
Scheme 1 Structures of Ponceau 4R (a) and Allura Red (b)

separation before analysis have caused more and more attention [16–22] for the substitution for the chromatographic [23] and spectroscopic methods [24].

Herein, graphene and ordered mesoporous TiO_2 were synthesized and characterized, respectively, and were used to prepare modified carbon paste electrode (CPE) for the first time. The electrochemical behaviors of Ponceau 4R and Allura Red on the surface of CPE, graphene-modified CPE (GN-CPE), mesoporous TiO_2-modified CPE (mesoporous TiO_2-CPE), and graphene/mesoporous TiO_2-modified CPE (GN/mesoporous TiO_2-CPE) were systematically studied. Interestingly, GN-CPE and mesoporous TiO_2-CPE gave rise to higher signals responding to Ponceau 4R and Allura Red oxidation relative to unmodified CPE, and further enhancement in peak current of Ponceau 4R and Allura Red oxidation was observed on GN/mesoporous TiO_2-CPE. Such enhancement effect might be attributed to increased surface area and improved accumulation efficiency for Ponceau 4R and Allura Red resulted from the modification of graphene and mesoporous TiO_2. Therefore, a novel electrochemical method for the detection of Ponceau 4R and Allura Red based on GN/mesoporous TiO_2-CPE was developed in this work, and the limit of detection of this method is much lower than the reported work (Table 1).

Experimental section

Reagents and instruments

Ponceau 4R, Allura Red, titanium butoxide ($Ti(OBu)_4$), hexadecyl trimethyl ammonium bromide (CTAB), graphite (Specpure), nano TiO_2 with solid structure, and other chemicals were purchased from the Sinopharm Group Chemical Reagent Co. Ltd., China with analytical grade purity. Ponceau 4R and Allura Red were dissolved into water to prepare 1.78×10^{-3} and 2.03×10^{-3} M standard stock solution, respectively, which were diluted by water to desired concentrations before use. The water used was redistilled.

Cyclic voltammetry (CV) and square wave voltammetry (SWV) were carried out with a CHI 660D electrochemical analyzer (Chenhua Instruments, China). A conventional three-electrode system, consisting of a GN/mesoporous TiO_2-CPE, a saturated calomel reference electrode (SCE), and a platinum wire auxiliary electrode, was employed.

Field emission scanning electron microscopy (SEM) was performed on Quanta 450 field emission scanning electron microscope (FEI, Holland). Transmission electron microscopy (TEM) images were obtained on TECNAI G2 20 S-TWIN transmission electron microscope (FEI, Holland). High-performance liquid chromatography (HPLC) determination was conducted on Agilent 1100 Series (USA).

Synthesis of graphene and mesoporous TiO_2

Graphene oxide was prepared from natural graphite flakes by Hummer's method [25] and was then reduced by $NaBH_4$ in a steam bath to produce the GN [26]. Mesoporous TiO_2 was synthesized according to the report [27], which used $Ti(OBu)_4$ as the source of Ti and CTAB as the organic template. The ordered mesopores could be formed in TiO_2 nanoparticles by calcining at 400 °C for 8 h to remove the organic template.

Preparation of the graphene and mesoporous TiO_2-modified CPE

Graphene (0.20 g), mesoporous TiO_2 or nano TiO_2 (0.20 g), and graphite powder (1.0 g) were exactly weighed and put in a carnelian mortar. The total mass ratio of graphene, mesoporous TiO_2 or nano TiO_2, and graphite was controlled to 1:1:5. After that, 0.35 mL paraffin oil was added into the powder and then mixed homogeneously. Finally, the resulting carbon paste was tightly pressed into the end cavity of electrode body, and the electrode surface was polished on a smooth paper, which was denoted as GN/mesoporous TiO_2-CPE or GN/nano TiO_2-CPE.

The GN-CPE and mesoporous TiO_2-CPE were prepared by the same procedure only using GN or mesoporous TiO_2, and the mass ratio of GN or mesoporous TiO_2 to graphite powder was fixed to 1:5. And the unmodified CPE was also prepared without addition of GN or mesoporous TiO_2.

Table 1 Comparison of the analytical performances between this work and the previously reported work

Analyte	Modified electrode	Linear range (μM)	Limit of detection (nM)	Reference
Ponceau 4R	Acetylene black nanoparticle/GCE	0.1~8.1	60.9	[16]
Ponceau 4R	Multi-wall carbon nanotube/GCE	0.051~3.05	30.5	[17]
Ponceau 4R	Bismuth film/GCE	20.1~101.5	2,030.9	[18]
Ponceau 4R	Graphene and mesoporous TiO_2/CPE	0.00406~0.20	1.35	This work
Allura Red	Multi-wall carbon nanotube/GCE	0.1~1.2	50.4	[17]
Allura Red	Polyallylamine/tubular electrode	10.0~150.0	1,400.0	[19]
Allura Red	Hanging mercury drop electrode	0.025~0.2	8.5	[20]
Allura Red	Graphene and mesoporous TiO_2/CPE	0.00067~0.21	0.34	This work

Analytical procedure

The 0.1-M H_2SO_4 was used as the supporting electrolyte for the detection of Ponceau 4R and Allura Red. After 4-min accumulation at 0.4 V, the square wave voltammograms were recorded from 0.4 to 0.95 V, and the oxidation peak current at 0.76 V was measured. The amplitude is 0.04 V, the frequency is 20 Hz, and the potential step increment is 5 mV.

Sample preparation and detection

Two soft drink and two sausage samples were purchased from a local market. The soft drink samples could be used directly without any pretreatment. The sausage samples needed to be treated as follows. Firstly, about 10.0 g of each sample was weighted, cut with a clean scissors, and grinded to uniform in a mortar. Then, the sample was put into a 100-mL beaker and mixed with 70 mL water and 12 mL 0.5 M NaOH. The pH of the solution was adjusted to 8.0 with NaOH and H_2SO_4 (both are 0.5 M) and then transferred to a 250-mL flask quantitatively following with 10.0 mL 0.42 M zinc sulfate was added to deposit protein. The flask was put in 60 °C water bath for 10 min, and adequate water was added to the mark when the flask was cooled to room temperature. It was kept still for 30 min. Whereafter, the fat floating above the solution was removed, and the residual solution was filtered. The first 50-mL filtrate was abandoned, and the subsequent filtrate was collected together and kept in refrigerator.

When detecting Ponceau 4R and Allura Red using a GN/mesoporous TiO_2-CPE, 0.1-mL sample solution was added into 5.0 mL 0.1 M H_2SO_4 and then analyzed according to the analytical procedure. When using HPLC system to assess Ponceau 4R and Allura Red, a C8 column (5 μm, 4.6×250 mm) was used as stationary phase, a mixture of 50 mM phosphate buffer at pH 7 containing Triton X-100 (0.25 %, v/v) was used as mobile phase, and a UV–visible Cintra 40 double-beam spectrophotometer was used as a detector [28].

Results and discussion

SEM and TEM images of graphene and mesoporous TiO_2

The morphology of graphene and mesoporous TiO_2 materials were characterized using SEM and TEM. From the SEM pictures, homogeneous, flexible, and wrinkled sheets were observed in image a, which represents the characteristic of graphene. However, mesoporous TiO_2 material represents as the aggregation of numerous TiO_2 nanoparticles with a diameter around 10 nm (b). A TEM image of mesoporous TiO_2 with low magnification is also shown in Fig. 1c. The morphology of the particles is shown as a mixture of a few of polygon. To probe the mesoporous architectures, a high-magnification TEM image is shown in Fig. 1d; the ordered mesopores of TiO_2 can be seen clearly, which not only greatly increase the effective surface area of this material, but also may play an important role in the redox process when used as electrode material.

Electrochemical response of GN/mesoporous TiO_2-CPE

The cyclic voltammetric behaviors of unmodified CPE, GN-CPE, mesoporous TiO_2-CPE, and GN/mesoporous TiO_2-CPE in 0.1 M KCl containing 5 mM $K_3[Fe(CN)_6]$ were studied. The redox peaks of $K_3[Fe(CN)_6]$ apparently improved at GN-CPE and mesoporous TiO_2-CPE compared to that at unmodified CPE, but the biggest oxidation peak current of $K_3[Fe(CN)_6]$ could be obtained at GN/mesoporous TiO_2-CPE, due to the strong accumulation and catalytic capacity of GN/mesoporous TiO_2 for $K_3[Fe(CN)_6]$. From the redox peaks of $K_3[Fe(CN)_6]$ at these four electrodes, the effective electrode surface area (A_e) can be calculated according to the Randles–Sevčík equation

$$I_p = (2.687 \times 10^5)n^{3/2}A_e D^{1/2}cv^{1/2} \qquad (1)$$

where n is the number of electrons transferred, D is the diffusion coefficient, c is the bulk concentration, and ν is the scan rate. It was found that the plots of peak current (I_p, A) of

Fig. 1 SEM images of graphene (**a**) and mesoporous TiO$_2$ (**b**). **c, d** TEM images of mesoporous TiO$_2$ with low and high magnification, respectively
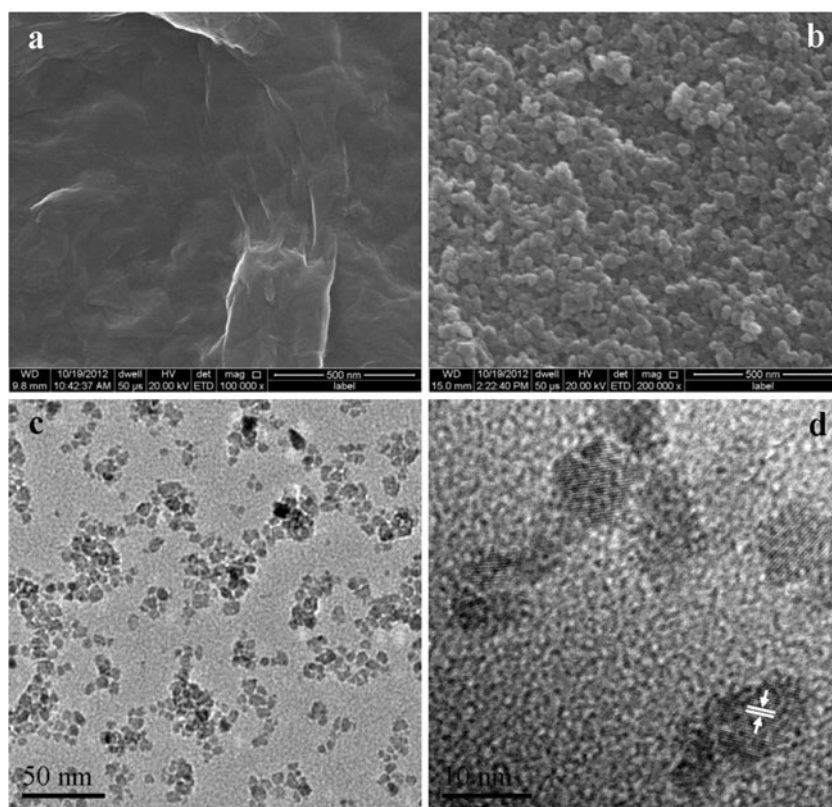
K$_3$[Fe(CN)$_6$] change linearly with $\nu^{1/2}$ (in volts per second) according to the regression that $I_p=(1.82\times10^{-6}\pm0.0204)+(2.45\times10^{-5}\pm0.0460)\nu^{1/2}$ ($r^2=0.996$) for unmodified CPE, $I_p=(7.32\times10^{-7}\pm0.0121)+(7.59\times10^{-5}\pm0.0272)\nu^{1/2}$ ($r^2=0.995$) for GN-CPE, $I_p=(5.11\times10^{-6}\pm0.0199)+(10.78\times10^{-5}\pm0.0247)\nu^{1/2}$ ($r^2=0.997$) for mesoporous TiO$_2$-CPE, and $I_p=(7.43\times10^{-6}\pm0.0215)+(2.09\times10^{-4}\pm0.0521)\nu^{1/2}$ ($r^2=0.998$) for GN/mesoporous TiO$_2$-CPE. A comparison of the slopes of the four electrodes reveals that the A_e of GN-CPE, mesoporous TiO$_2$-CPE, and GN/mesoporous TiO$_2$-CPE is 3.1-fold, 4.4-fold, and 8.5-fold larger than that of unmodified CPE, respectively, which shows that the modification of graphene and mesoporous TiO$_2$ on CPE can obviously enlarge the surface area and therefore improve the accumulation ability of GN/mesoporous TiO$_2$-CPE to analytes.

Electrochemical behaviors of Ponceau 4R and Allura Red

The electrochemical behaviors of Ponceau 4R on unmodified CPE and GN/mesoporous TiO$_2$-CPE were studied using CV. Figure 2 shows the CV curves of 1.0 μM Ponceau 4R in 0.1 M H$_2$SO$_4$. During the first anodic sweep from 0.5 to 1.0 V, an oxidation peak at 0.814 V was observed on the unmodified CPE surface (curve a). On the reverse scan from 1.0 to 0.5 V, a corresponding reduction peak appeared at 0.79 V, suggesting that the electrochemical process of Ponceau 4R is a whole redox reaction. The reduction peak current of Ponceau 4R on

the second cycle became somewhat bigger, which is almost equal to the oxidation peak current of Ponceau 4R; therefore, the second cyclic behavior of Ponceau 4R is more symmetrical than the first one, which may be caused by the adsorption of Ponceau 4R on unmodified CPE. Under the identical conditions, a pair of well-defined redox peaks was revealed in the first cycle at GN/mesoporous TiO$_2$-CPE (curve b), and the difference between oxidation peak potential and reduction
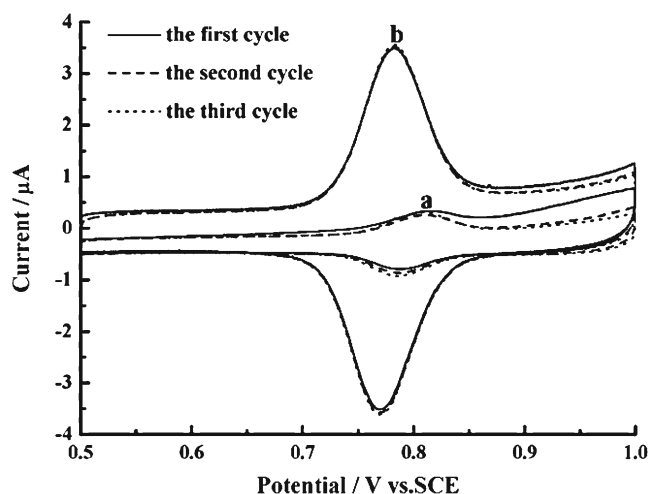

Fig. 2 CV curves of 1.0 μM Ponceau 4R in 0.1 M H$_2$SO$_4$ on unmodified CPE (*a*) and GN/mesoporous TiO$_2$-CPE (*b*). Scan rate is 100 mV s^{-1}

peak potential (ΔE_p) is much smaller than that on the unmodified CPE, suggesting a more fast electron transfer of Ponceau 4R at GN/mesoporous TiO$_2$-modified CPE. During the following cyclic sweeps, the redox peak current did not decrease at all, indicating the GN/mesoporous TiO$_2$-CPE could be used repeatedly and may have good anti-contamination ability against the electrochemical reaction product of Ponceau 4R. Besides, the peak current of Ponceau 4R increased evidently compared with that on unmodified CPE, which is caused by the strong enhancement effect of graphene and mesoporous TiO$_2$.

The electrochemical behaviors of 1.0 μM Allura Red in 0.1 M H$_2$SO$_4$ at unmodified CPE and GN/mesoporous TiO$_2$-CPE were also investigated (Fig. 3). Clearly, one oxidation peak (O1) appeared in the first cycle with the peak potential (E_p) at 0.93 V (curve a). A strong reduction peak (R1) at 0.92 V appeared in the reverse sweep, which was caused by the reduction reaction of the product of peak O1. And a weak reduction peak (R2) at 0.75 V appeared subsequently. In the second cycle, a new weak oxidation peak (O2) located at 0.76 V was observed, which formed a redox couple with peak R2. And the notable peak current decline for redox couple O1/R1 could be seen on the second and third cycles, which may attribute to the strong adsorption of redox products, which could cause the contamination and passivation of the GN/mesoporous TiO$_2$-CPE surface. Interestingly, when the potential sweep ends at 0.85 V, a potential giving no chance for the peak O1 to oxidize, peak R2 completely disappears (curve b), and consequently, the disappearance of peak O2 in the second and third cycles. This result suggests that peak R2 is related to the oxidation of the product of peak O1. The possible mechanism of electrochemical redox for Allura Red at GN/mesoporous TiO$_2$-CPE is shown in Scheme 2 based on literature [29, 30]. The
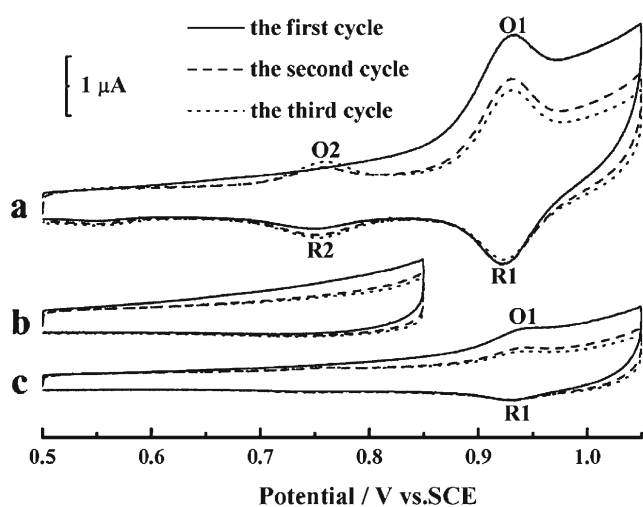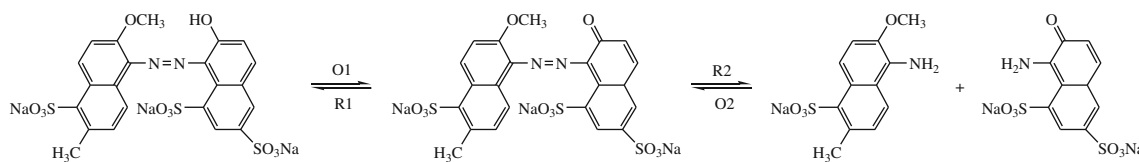
voltammograms of Allura Red at unmodified CPE were much different (curve c), i.e., the redox couple R2/O2 for 1.0 μM Allura Red disappeared. And the peak current of the redox couple O1/R1 decreased about three times compared with the GN/mesoporous TiO$_2$-CPE, which further testifies the high activity and accumulation efficiency of GN/mesoporous TiO$_2$-CPE to the analyte attributing to the large surface area and strong catalytic ability of graphene and mesoporous TiO$_2$. It can be seen from the above that the peak O1 in the first scan is the most sensitive one of these peaks, so it is chosen as the analytical signal for Allura Red in the following study.

The electrochemical responses of low-concentration Ponceau 4R at unmodified CPE, GN-CPE, mesoporous TiO$_2$-CPE, GN/mesoporous TiO$_2$-CPE, and GN/nano TiO$_2$-CPE were investigated using SWV because it is a highly sensitive analytical technique. Figure 4 depicts the SWV responses of Ponceau 4R in 0.1 M H$_2$SO$_4$. At the unmodified CPE, a very weak oxidation peak with a peak current of 0.63 μA was observed at 0.78 V for 0.1 μM Ponceau 4R even after 4-min accumulation (curve a), suggesting that the oxidation activity of Ponceau 4R is very poor at the unmodified CPE surface. However, an evident oxidation peak appeared at 0.77 V on GN-CPE (I_p=2.8 μA) (curve b), and a more sensitive oxidation peak appeared at 0.76 V with a bigger peak current of 7.0 μA at mesoporous TiO$_2$-CPE (curve c). When graphene and mesoporous TiO$_2$ were both used to modify CPE, the peak current of 0.1 μM Ponceau 4R achieved the biggest value, i.e., 11.0 μA (curve d), which attributes to the synergistic effects of graphene and mesoporous TiO$_2$. Furthermore, the SWV curves of unmodified CPE (curve e) and GN/mesoporous TiO$_2$-CPE (curve f) in 0.1 M H$_2$SO$_4$ were smooth without any evident peak, indicating the attribution of the oxidation peak to Ponceau 4R. Additionally, commercial nano TiO$_2$ particles with solid structure were also used to modify CPE. It was found that the oxidation peak current of Ponceau 4R at GN/nano TiO$_2$-CPE (curve g) is much lower than that at GN/mesoporous TiO$_2$-CPE (inset of Fig. 4), which confirms the superior accumulation ability of the mesopores in TiO$_2$ particles.

The responses of Allura Red oxidation on different electrodes were also compared using SWV in 0.1 M H$_2$SO$_4$. As shown in Fig. 5, an oxidation peak at 0.91 V was observed on CPE surface after 4-min accumulation (I_p=1.68 μA, curve a). On the surface of GN-CPE (curve b) and mesoporous TiO$_2$-CPE (curve c), the oxidation peak current of Allura Red greatly increased to 5.6 and 7.3 μA, respectively, indicating the high activity of graphene and mesoporous TiO$_2$. Importantly, the oxidation signal of Allura Red further enhanced obviously on the surface of GN/mesoporous TiO$_2$-CPE at 0.89 V (I_p=12.3 μA, curve d). Apparently, graphene and mesoporous TiO$_2$ exhibit a remarkable enhancement effect toward the oxidation of Allura Red when they coexist. Furthermore, the SWV signal of Allura Red at GN/nano TiO$_2$-

Fig. 3 CV curves of 1.0 μM Allura Red in 0.1 M H$_2$SO$_4$ on unmodified CPE (*c*) and GN/mesoporous TiO$_2$-CPE (*a*) from 0.5 to 1.05 V. *Curve b* depicts 1.0 μM Allura Red on GN/mesoporous TiO$_2$-CPE from 0.5 to 0.85 V. Scan rate is 100 mV s^{-1}

Scheme 2 The possible mechanism of electrochemical redox for Allura Red at GN/mesoporous TiO$_2$-CPE

CPE (curve g) is weaker than that at GN/mesoporous TiO$_2$-CPE (inset of Fig. 5). This may be because the mesopores of nano-scale TiO$_2$ particles have served as channels for the electron transfer of Allura Red. And the presence of graphene provides enough mechanical strength for the support of mesoporous TO$_2$ nanoparticles. In addition, the SWV curves on unmodified CPE (curve e) and GN/mesoporous TiO$_2$-CPE (curve f) in the absence of Allura Red were virtually feature-less, suggesting that the peak at about 0.89 V is most likely due to Allura Red oxidation.

Optimizing of some experimental parameters

The optimum of the supporting electrolyte

The electrochemical behaviors of 1.0 μM Ponceau 4R and Allura Red were examined in different supporting electrolytes such as disodium hydrogen phosphate–citric acid buffer solution (pH 2.2, 3.6, 4.4, 7.0, and 8.0), 0.2 M sodium acetate–acetic acid buffer solution (pH 2.6, 4.0, 4.4, and 5.4), boric acid–borax buffer solution (pH 7.4, 8.0, 8.4, and 9.0), 0.1 M phosphate buffer solution (pH 5.8, 6.5, 7.0, and 8.0), and 0.1 M HCl, H$_2$SO$_4$, HClO$_4$, and NaOH solution by CV. It was found that the oxidation peak current of Ponceau 4R and Allura Red became the highest in 0.1 M H$_2$SO$_4$ and the voltammogram

shapes were well defined. So, 0.1 M H$_2$SO$_4$ was chosen as the electrolyte for the electrochemical oxidation of Ponceau 4R and Allura Red.

The optimum of the content of graphene and mesoporous TiO$_2$

The influences of mass content of graphene and mesoporous TiO$_2$ on the oxidation peak current of Ponceau 4R and Allura Red were investigated. When changing the mass ratio of graphene/mesoporous TiO$_2$/graphite from 1:1:7, 1:1:6, 1:1:5, 1:1:4, 1:2:5, 1:3:5, and 2:1:5 to 3:1:5, the highest peak could be obtained when the mass ratio is 1:1:5. Less graphene and mesoporous TiO$_2$ content may reduce the effective electrode surface area, which may weaken the accumulation ability of GN/mesoporous TiO$_2$-CPE. However, more graphene and mesoporous TiO$_2$ content may lower the conductivity of the modified electrode, which may hinder the electron transfer of Ponceau 4R and Allura Red. So, the mass ratio of graphene/mesoporous TiO$_2$/graphite was chosen as 1:1:5.

The optimum of accumulation potential and time

The oxidation peak current of Ponceau 4R and Allura Red under open circuit and different accumulation potentials
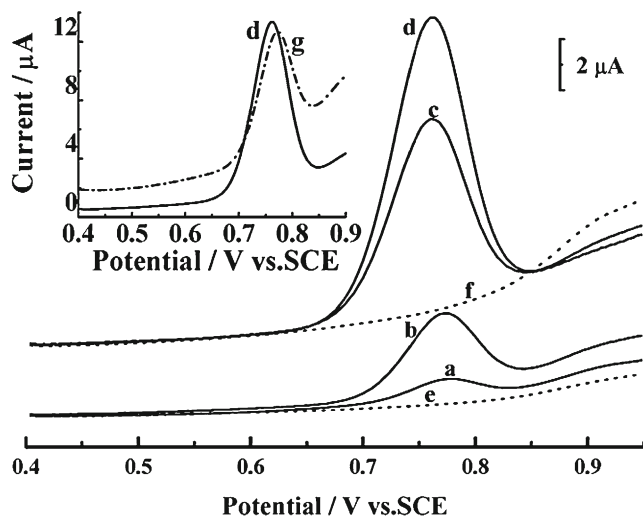

Fig. 4 SWV curves of 0.1 μM Ponceau 4R at CPE (*a*), GN-CPE (*b*), mesoporous TiO$_2$-CPE (*c*), GN/mesoporous TiO$_2$-CPE (*d*), and GN/nano TiO$_2$-CPE (*g*) in 0.1 M H$_2$SO$_4$. Curves *e* and *f* correspond to unmodified CPE and GN/mesoporous TiO$_2$-CPE in 0.1 M H$_2$SO$_4$, respectively. Accumulation time is 4 min
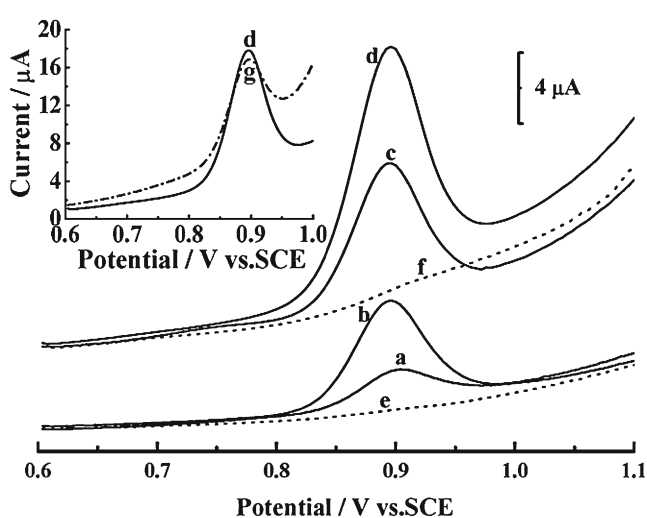

Fig. 5 SWV curves of 0.03 μM Allura Red at CPE (*a*), GN-CPE (*b*), mesoporous TiO$_2$-CPE (*c*), GN/mesoporous TiO$_2$-CPE (*d*), and GN/nano TiO$_2$-CPE (*g*) in 0.1 M H$_2$SO$_4$. Curves *e* and *f* correspond to unmodified CPE and GN/mesoporous TiO$_2$-CPE in 0.1 M H$_2$SO$_4$, respectively. Accumulation time is 4 min

Table 2 Influence of other compounds on the peak current of 0.05 μM Ponceau 4R and Allura Red in 0.1 M H_2SO_4 at GN/mesoporous TiO_2-CPE

Interferents	Concentration (μM)	Signal change for Ponceau 4R (%)	Signal change for Allura Red (%)
Glucose	50	0.68	0.43
Sucrose	50	0.40	−0.28
Glycine	50	0.56	0.37
Citric acid	25	−0.44	0.54
Vitamin C	12.5	0.61	0.38
Fe^{3+}	5	0.52	0.40
Fe^{2+}	5	0.17	0.55
Ca^{2+}	5	−0.63	−0.39
Cu^{2+}	5	0.72	0.52
Sunset yellow	0.5	0.75	−0.22
Tartrazine	0.5	0.53	0.47
Quinoline yellow	0.5	−0.29	0.26

from 0.2 to 0.8 V were individually measured to evaluate the influence of accumulation potential. The oxidation peak current of Ponceau 4R and Allura Red kept constant, revealing no influence of accumulation potential on the detection of Ponceau 4R and Allura Red. Therefore, the initial potential, i.e., 0.4 V for Ponceau 4R and 0.6 V for Allura Red, was applied during their accumulation steps.

The dependence of the oxidation peak current of Ponceau 4R and Allura Red on accumulation time was also tested at the GN/mesoporous TiO_2-CPE. The oxidation peak current of 1 μM Ponceau 4R and Allura Red increased quickly from 0 to 120 s and slowly from 120 to 240 s. At an accumulation time of 240 s, the peak current of Ponceau 4R and Allura Red both achieved the zenith. The calibration curves gradually tend to plateau when the accumulation time increased further, indicating that the adsorption of Ponceau 4R and Allura Red on GN/mesoporous TiO_2-CPE is saturated. As a result, the accumulation time of 240 s was selected for the experiment.

Influence of scan rate

The influences of scan rate on the oxidation current of Ponceau 4R and Allura Red on GN/mesoporous TiO_2-CPE were examined in the range of 10–800 mV s^{-1}. The results showed that the oxidation peak current of Ponceau 4R and Allura Red linearly increased with the scan rate, indicating their adsorption-controlled electrode processes. Meanwhile, the oxidation peak potential (E_p, in volt) of Ponceau 4R and Allura Red positively shifted with scan rate (ν, in millivolts per second) according to the regression of $E_p = (1.201 \pm 0.0460) + (0.0417 \pm 0.0236) \ln \nu$ ($r^2 = 0.997$) for Ponceau 4R and $E_p = (0.998 \pm 0.0799) + (0.0472 \pm 0.0220) \ln \nu$ ($r^2 = 0.999$) for Allura Red; so, both of them take place an irreversible electrochemical process. For an irreversible and adsorption-controlled electrode process, the relationship between E_p (in volt) and ν (in millivolts per second) is in accordance with the following equation [31]:

$$E_p = E^{0'} + \left(\frac{RT}{\alpha nF}\right) \ln \left(\frac{RTk^0}{\alpha nF}\right) + \left(\frac{RT}{\alpha nF}\right) \ln \nu \qquad (2)$$

where k^0 is the standard rate constant of the surface reaction, $E^{0'}$ is the formal potential, α is transfer coefficient of the oxidation of Ponceau 4R or Allura Red, and other symbols have their usual meanings. According to Eq. (2), the plot of E_p vs. $\ln \nu$ has a good linear relationship, from which αn can be determined from the slope (i.e., 0.0417 for Ponceau 4R and 0.0472 for Allura Red). Assuming $\alpha = 0.5$, one electron was involved in both of the oxidation of Ponceau 4R and Allura Red, occurring at their phenolic hydroxyl group.

Calibration, reproducibility, and anti-interference capacity

Under the optimal working conditions, the calibration plots for Ponceau 4R and Allura Red in 0.1 M H_2SO_4 at GN/mesoporous TiO_2-CPE were characterized by SWV. It was found that the SWV oxidation peak current increased with increasing Ponceau 4R or Allura Red concentration. The oxidation current of

Table 3 Determination of Ponceau 4R and Allura Red in soft drink (nos. 1 and 2) and sausage (nos. 3 and 4) samples by six parallel replicates

No.	Analytes	By this method (nM)	By HPLC (nM)	Relative error (%)	t value	F value	Added (nM)	Found (nM)	Recovery (%)[a]
1	Ponceau 4R	17.32±0.03	17.81±0.04	−2.8	0.74	2.14	20.00	19.74±0.02	98.70±2.3
	Allura Red	0.00	0.00				20.00	20.15±0.05	100.8±2.3
2	Ponceau 4R	0.00	0.00				25.00	24.76±0.04	99.04±2.2
	Allura Red	24.24±0.03	23.98±0.03	1.1	0.52	1.34	25.00	25.41±0.06	101.6±2.5
3	Ponceau 4R	5.19±0.05	5.08±0.02	2.2	0.61	1.87	5.00	4.87±0.03	97.40±2.6
	Allura Red	0.00	0.00				5.00	5.11±0.05	102.2±2.5
4	Ponceau 4R	7.43±0.09	7.59±0.07	−2.1	0.55	2.06	8.00	8.23±0.03	102.9±2.7
	Allura Red	0.00	0.00				8.00	7.77±0.10	97.12±2.2

[a] Average of six measurements±standard deviation

Ponceau 4R is proportional to its concentration from 4.06 nM to 0.20 μM with a detection limit of 1.35 nM (I_p=(0.258±0.0167)+(0.103±0.00193) c, r^2=0.999). And the oxidation current of Allura Red is proportional to its concentration in the range of 0.67 nM to 0.21 μM with a detection limit of 0.34 nM (I_p=(1.134±0.0446)+(0.286± 0.00696) c, r^2=0.997).

The successive measurements using one GN/mesoporous TiO_2-CPE were examined. The oxidation peak current of Ponceau 4R kept unchanged. Thus, GN/mesoporous TiO_2-CPE can be used repeatedly for the determination of Ponceau 4R, and the relative standard deviation (RSD) is 2.3 % for ten measurements on the same GN/mesoporous TiO_2-CPE. Unfortunately, the oxidation peak current of Allura Red decreased continuously, most likely due to the strong surface adsorption of the oxidation product of Allura Red. So, GN/mesoporous TiO_2-CPE can only be employed just for single measurement for Allura Red. The repeatability between ten GN/mesoporous TiO_2-CPE was then evaluated by parallel determination of the oxidation peak current of 0.1 μM Ponceau 4R or Allura Red. The RSD is 3.2 and 3.7 % for Ponceau 4R and Allura Red, respectively, indicative of an excellent fabrication reproducibility and detection precision.

Various possible interferents were tested to assess their influences on the determination of Ponceau 4R and Allura Red (Table 2). Interference studies were conducted by exposing GN/mesoporous TiO_2-CPE to 0.05 μM Ponceau 4R or Allura Red in 0.1 M H_2SO_4 containing interferents at certain concentrations. The results show that 1,000-fold glucose, sucrose, and glycine; 500-fold citric acid; 250-fold vitamin C; 100-fold Fe^{3+}, Fe^{2+}, Ca^{2+}, and Cu^{2+}; or 10-fold sunset yellow, tartrazine, and quinoline yellow has no interference on the determination of Ponceau 4R and Allure Red (the peak current change is below 8 %). However, twofold amaranth interferes the determination of Ponceau 4R, and equivalent concentration of amaranth interferes the determination of Allura Red seriously.

Analytical application

In order to ascertain its potential application, this newly developed method was employed to detect Ponceau 4R and Allura Red in soft drink (nos. 1 and 2) and sausage (nos. 3 and 4) samples. The results obtained by the standard addition method using GN/mesoporous TiO_2-CPE are shown in Table 3. In order to test the accuracy of this method, the contents of Ponceau 4R and Allura Red were also analyzed by HPLC. The results obtained by HPLC and the GN/mesoporous TiO_2-CPE are in good agreement with an acceptable recovery percentage (97±2.7 %, n=6). Furthermore, the F and t tests at 95 % confidence levels did not exceed the tabulated (theoretical) ones and no significant differences were observed between the developed and the HPLC methods with respect to precision and accuracy, revealing that this method is effective and reliable. In addition, known amounts of Ponceau 4R or Allura Red were spiked in the samples, respectively, and then analyzed according to the same procedure. The value of recovery percentage (97.12–102.9±2.5 %) is satisfied, also indicating that this method is accurate and feasible.

Conclusions

In this work, the electrochemistry of Ponceau 4R and Allura Red on graphene/mesoporous TiO_2-modified CPE (GN/mesoporous TiO_2-CPE) was first investigated. Compared with CPE, graphene-modified CPE and TiO_2-modified CPE, GN/mesoporous TiO_2-CPE remarkably enhanced the oxidation peak current of Ponceau 4R and Allura Red, most likely due to a larger surface area and a stronger accumulation efficiency toward Ponceau 4R and Allura Red. The scan rate effect on Ponceau 4R and Allura Red at the GN/mesoporous TiO_2-CPE indicated that a one-electron process took place in both of them, occurring at their phenolic hydroxyl group. Based on the notable enhancement effect of graphene and mesoporous TiO_2, a sensitive, rapid, and simple electrochemical method was developed for the detection of Ponceau 4R and Allura Red.

References

1. Geim AK, Novoselov KS (2007) Nat Mater 6:183–191
2. Katneson MI (2007) Mater Today 10:20–27
3. Yang T, Liu LH, Jia JW (2012) J Mater Chem 22:21909–21916
4. Beidaghi M, Wang CL (2012) Adv Funct Mater 22:4501–4510
5. Gan T, Sun JY, Cao SQ, Gao FX, Zhang YX, Yang YQ (2012) Electrochim Acta 74:151–157
6. Cheng YF, Yuan R, Chai YQ (2012) Anal Chim Acta 745:137–142
7. Lian WJ, Liu S, Yu JH (2012) Biosens Bioelectron 38:163–169
8. Xi Q, Chen X, Evans DG, Yang WS (2012) Langmuir 28:9885–9892
9. Gan T, Sun JY, Huang KJ, Li YM (2013) Sens Actuator B-Chem 177:412–418
10. Kresge CT, Leonowicz ME, Roth WJ, Vartuli JC, Beck JS (1992) Nature 359:710–712
11. Beck JS, Vartuli JC, Roth WJ, Leonowicz ME, Kresge CT, Schmitt KD, Chu CTW, Olsen DH, Sheppard EW, McCullen SB, Higgins JA, Schlenker JL (1992) J Am Chem Soc 114:10834–10843
12. Wagner T, Sauerwald T, Kohl CD, Waitz T, Weidmann C, Tiemann M (2009) Thin Solid Films 517:6170–6175
13. Tiemann M (2007) Chem-Eur J 13:8376–8388
14. Hagfeldt A, Graetzel M (1995) Chem Rev 95:49–68
15. Vidotti EC, Costa WF, Oliveira CC (2006) Talanta 68:516–521

16. Yang XF, Qin HB, Gao MM, Zhang HJ (2010) J Agr Food Chem 91:2821–2825
17. Zhang Y, Zhang XJ, Lu XH, Yang JQ, Wu KB (2010) Food Chem 122:909–913
18. Claux B, Vittori O (2007) Electroanalysis 19:2243–2246
19. Silva MLS, Garcia MBQ, Lima JLFC, Barrado E (2007) Talanta 72:282–288
20. Alghamdi AH (2005) J AOAC Int 88:1387–1393
21. Wang JQ, Wu C, Wu KB, Cheng Q, Zhou YK (2012) Anal Chim Acta 736:55–61
22. Cheng Q, Wu C, Chen JW, Zhou YK, Wu KB (2011) J Phys Chem C 115:22845–22850
23. Khanavi M, Hajimahmoodi M, Ranjbar AM, Oveisi MR, Ardekani MRS, Mogaddam G (2012) Food Anal Method 5:408–415
24. Soylak M, Unsal YE, Tuzen M (2011) Food Chem Toxicol 49:1183–1187
25. Sreeprasad TS, Samal AK, Pradeep T (2009) J Phys Chem C 113:1727–1737
26. Bourlinos AB, Gournis D, Petridis D, Szabó T, Szeri A, Dékány I (2003) Langmuir 19:6050–6055
27. Li XK, Zhuang ZJ, Li W, Pan HQ (2012) Appl Catal A-Gen 429–430:31–38
28. Mahnaz K, Mannan H, Ali MR, Mohammad RO, Mohammad RSA, Ghazaleh M (2012) Food Anal Method 5:408–415
29. Yu JF, Jia JP, Ma ZF (2004) J Chin Chem Soc 51:1319–1324
30. Medeiros RA, Lourencao BC, Rocha-Filho RC, Fatibello-Filho O (2012) Talanta 97:291–297
31. Laviron E (1974) J Electroanal Chem 52:355–393